Journal of Superconductivity and Novel Magnetism (2024) 37:1141–1151
https://doi.org/10.1007/s10948-024-06702-z

RESEARCH

Study on the Influence of Annealing and Ball Milling on the Magnetic Properties of HDDR Nd-Fe-B Magnetic Powder

Chao Liang[1] · Min-gang Zhang[1,2] · Feng-hua Chen[1] · Wen-feng Liu[1] · Yong-an Dong[3]

Received: 29 November 2023 / Accepted: 26 January 2024 / Published online: 18 March 2024

Abstract

The Nd-Fe-B anisotropic magnetic powders were subjected to tempering and ball milling processes. Analysis of the magnetic properties, structure, and physical phase revealed that the following: the integrated magnetic properties of the magnetic powder were the best when the tempering temperature and time were separately 650 °C and 20 min, for DOA = 0.73, B_r = 6.547 kGs, H_{cj} = 12.255 kOe, and $(BH)_{max}$ = 7.117 MGOe. When the DR temperature is 860 °C, the tempering temperature is 650 °C, and the tempering time is 20 min, the ideal magnetic properties of the magnetic powder are DOA = 0.69, B_r = 6.238 kGs, H_{cj} = 14.67 kOe, and $(BH)_{max}$ = 7.060 MGOe. The integrated magnetic properties of the magnetic powders were optimal when the ball milling speed, time, and doped Cu content were 350 rpm, 2 h, and 10 wt%, for DOA = 0.62, B_r = 4.96 kGs, H_{cj} = 9.86 kOe, and $(BH)_{max}$ = 4.39 MGOe. The ideal tempering temperature and time can promote the diffusion of Nd-rich phase to the grain boundaries, strengthen the pinning effect on the magnetic domains, and improve the coercivity of the magnetic powder. The ideal ball milling speed and time can effectively reduce the particle size of the main phase particles of the magnetic powder and the large particles of the Nd-rich phase, so that the Nd-rich phase is uniformly distributed at the grain boundaries, to achieve the effect of de-magnetization coupling and improve the coercivity of the magnetic powder. After ball milling the magnetic powder doped with an appropriate amount of Cu powder, Cu induces the precipitation of a certain amount of Nd in the main phase of $Nd_2Fe_{14}B$. This Nd is uniformly distributed at the grain boundaries, achieving the effect of repairing the grain boundaries, thereby improving the coercivity of the magnetic powder.

Keywords Nd-Fe-B magnetic powder · Temper · Ball mill · Anisotropy

1 Introduction

Nd-Fe-B magnets, as the third generation of rare earth permanent magnet, are essentially functional that support the development of and technological innovation in modern society. They are widely used in aviation [1], network communication [2], transportation [3, 4], intelligence [5], and other technology fields, utilizing magnetic physics effects and the function of magnetic energy interconversion with other forms of energy [6]. Nd-Fe-B magnetic powder, as the superior raw material for preparing sintered and bonded Nd-Fe-B magnets, plays a decisive role in the magnetic properties of the sintered and bonded Nd-Fe-B magnets [7, 8]. Currently, we are in an era of rapid development of science and technology, and the proportion of rare earth resources is gradually declining. Therefore, it is significant to study how to improve the utilization rate of Nd elements in Nd-Fe-B magnetic powders. This can not only reduce the waste of rare earth resources but also extend the economic life cycle of

✉ Min-gang Zhang
am_lab@yeah.net

Chao Liang
liangchaoleesin@163.com

Feng-hua Chen
2001005@tyust.edu.cn

Wen-feng Liu
2006047@tyust.edu.cn

Yong-an Dong
1871624525@qq.com

[1] School of Materials Science and Engineering, Taiyuan University of Science and Technology, Taiyuan 030024, China

[2] Upgrading Office of Modern College of Humanities and Sciences, Shanxi Normal University, Linfen 041000, China

[3] Taiyuan Blooming Source Permanent Magnet Equipment Co. Ltd., Taiyuan 030003, China

enterprise products [9]. There are three main process methods to improve the utilization rate of Nd in NdFeB magnetic powder or to reduce the use of rare earth elements: grain boundary diffusion [10–12], grain refinement [13–15], and granular phase structure adjustment [16–18].

Yu et al. [19] studied the effect of-temperature tempering + low-temperature tempering on sintered NdFeB magnets. The results show that the magnet possesses higher H_{cj} but lower B_r after high-temperature tempering, on which low-temperature tempering can effectively improve the magnetic properties. The high-temperature tempering can make the non-uniform phase in the main phase disappear, the grain boundaries become clear and smooth, and the H_{cj} is greatly improved. Song [20] investigated the effect of using a secondary tempering process on the magnetic properties of magnets. The study showed that the secondary tempering process can improve the microstructure of sintered Nd-Fe-B. The low-temperature tempering not only prevents the growth of the main phase grains but also enables the smooth formation of the liquid phase between the main phase grains. Yue et al. [21] found that proper tempering of Nd-Fe-B magnetic powder was beneficial to the improvement of material coercivity, but no specific analysis of other magnetic properties of Nd-Fe-B magnetic powder and microstructure was carried out.

An et al. [22] systematically investigated the effect of milling temperature on the crystal structure, morphology, and magnetic properties of prepared Nd-Fe-B powders. The Nd-Fe-B powders milled at room temperature and low temperature showed obvious differences in morphology. Wang [23] utilized a ball mill to mill a mixture of NdFeB oxides reductants and observed significant increase in the coercivity H_{cj} and remanent magnetization B_r. The enhancement of the properties is mainly attributed to the refinement of the $Nd_2Fe_{14}B$ main phase grains, the increase in the degree of anisotropic orientation, and the magnetic exchange coupling of the $Nd_2Fe_{14}B$ main phase with nanoscale α-Fe. Research has also indicated [24] that adding small amounts of Cu to magnetic powders can heighten their coercivity. The mechanism behind this involves Cu being primarily distributed in the corners of grain boundaries to facilitate the repair of said boundaries and demagnetization coupling. In another study, Hussain et al. [25] examined the impact of different ball milling durations on the magnetic properties of nanocrystalline alloys, concluding that the optimal magnetic properties were achieved when the powder was milled for 80 min.

At present, studies on enhancing the magnetic properties of Nd-Fe-B powders have focused on optimizing the HDDR (hydrogen-disproportionation-dehydrogenation-recombination) process parameters for the preparation of Nd-Fe-B powders [15], as well as the optimization of tempering process parameters after sintering into Nd-Fe-B magnets [26, 27]. However, limited work has been conducted on improving the magnetic properties of Nd-Fe-B magnetic powders prepared by the HDDR process. Consequently, this study aims to enhance the magnetic properties, especially the coercivity, of anisotropic Nd-Fe-B magnetic powders prepared through HDDR, utilizing tempering heat treatment and ball milling processes. This research investigates the effects of different tempering heat treatment and ball milling process parameters on the microstructure and magnetic properties of magnetic powders, aiming to identify the optimal process parameters.

2 Experiment

The ingot alloy with a composition of $Nd_{14.3}Pr_{0.06}Fe_{78.64}B_7$ used to prepare Nd-Fe-B magnetic powder through the d-HDDR (dynamic-HDDR) process. The magnetic properties the powder were enhanced through tempering heat treatment and ball milling treatment. The process steps are as follows:

1. Tempering process: place the magnetic powder into a dry quartz tube, and secure it using a vacuum quartz tube sealing machine. Utilize a vacuum application equipment machine to evacuate and fill the tube with high purity argon gas, repeating the process 2 to 3 times until the vacuum in the quartz tube reaches less than 1×10^{-2} Pa. Fill the tube with 20 MPa argon gas, and seal it using a hydroxide flame fusion sealing machine. Place the quartz tube in an energy-saving chamber furnace, and heat it to 600 ~ 700 ℃, maintaining the temperature for 10 ~ 30 min. Afterward, remove the tube, and allow it to air-cool to room temperature. The comprehensive magnetic performance of the magnetic powder before tempering is as follows: DOA = 0.73, B_r = 6.61 kGs, H_{cj} = 8.20 kOe, and $(BH)_{max}$ = 5.69 MGOe.
2. Ball milling process: in a glove box environment filled with argon gas, pour the magnetic powder and steel beads into the ball milling jar and seal it. Then, evacuate the jar using a vacuum application equipment machine; fill it with high purity argon gas, repeating the process 2 ~ 3 times to achieve a vacuum level in the ball milling jar of less than 1×10^{-2} Pa. Use the planetary ball mill to mill for 1 ~ 3 h under fixed rotation and a rotation speed of 150 ~ 350 rpm. The comprehensive magnetic performance of the magnetic powder before milling is as follows: DOA = 0.54, B_r = 4.90 kGs, H_{cj} = 4.70 kOe, and $(BH)_{max}$ = 2.87 MGOe.

Based on existing studies in our group [28, 29], the amount magnetic powder prepared using the best d-HDDR process parameters was too small to meet the required amount for this study. Therefore, the ideal tempering and ball milling process parameters were first explored using magnetic powder with poor performance. Subsequently, the magnetic properties of the best-performing magnetic powder were improved under these process conditions.

The magnetic properties were tested using Quantum Design's VL015 vibrating sample magnetometer (VSM), surface morphology was observed using Hitachi S-4800 scanning electron microscope (SEM), and composition analysis was conducted using the DX2700B model X-ray diffractometer (XRD) from Shanghai Precision Instruments Co. The Plus software program was utilized to refine and fit the XRD patterns, and the relative contents of different phases in the magnetic powder were calculated.

3 Results and Discussion

3.1 Effect of Tempering on the Structure and Magnetic Properties of Nd-Fe-B Magnetic Powder

Figure 1 depicts the variation curves of magnetic properties of magnetic pow after tempering at temperatures of 600 °C, 650 °C, 700 °C, 750 °C, and 800 °C, with a tempering time of 20 min. As illustrated in Fig. 1, the remanent magnetization of the powder decreases after the tempering heat treatment. With the increase of tempering temperature, the coercivity of the magnetic powder first increases and then decreases. The initial increase is attributed to the greater driving force for atomic diffusion at higher tempering temperatures, resulting in fuller and more uniform atomic diffusion and a more even distribution of Nd-rich phases at the grain boundaries, thereby achieving de-magnetization and coupling effects and improving the coercivity of the magnetic powder. The subsequent reduction occurs because excessive tempering temperature causes abnormal growth of the main phase particles, leading to compositional segregation during the cooling process and resulting in a decrease in the coercivity of the magnetic powder. The maximum magnetic energy product of the powder demonstrates an initial increase followed by a decrease with the rise in tempering temperature. The degree of anisotropic orientation of the magnetic powder is indicated by DOA, where DOA = M_r/M_s. An anisotropic magnetic powder is denoted by DOA > 0.5 [6]. As the tempering temperature increases, DOA initially decreases, followed by an increase and then a decrease without displaying a clear trend. In summary, the coercivity of magnetic powder is maximum at the tempering temperature of 650 °C, and its ideal integrated magnetic properties are DOA = 0.73, B_r = 6.547 kGs, H_{cj} = 12.255 kOe, and $(BH)_{max}$ = 7.117 MGOe.

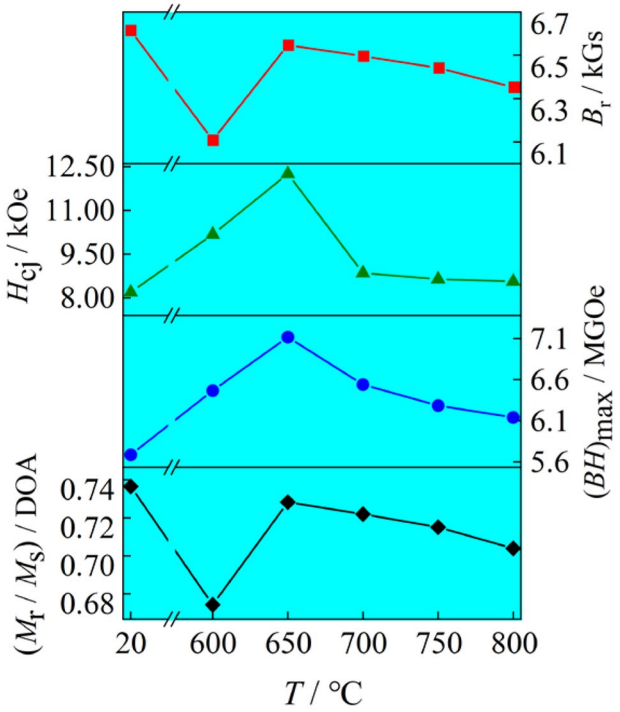

Fig. 1 Magnetic property change curve of magnetic powder at different tempering temperatures

Figure 2a–f displays the SEM photographs of the untempered powders and the magnetic powders after tempering for 20 min at 600 °C, 650 °C, 700 °C, 750 °C, and 800 °C. The main phase particles of $Nd_2Fe_{14}B$ in Fig. 2a are seen to be accompanied by a large number of Nd-rich white particles. This presence of a large number of Nd-rich white particles attached to the main-phase particles of $Nd_2Fe_{14}B$ reduces the Nd content at the grain boundaries, resulting in decreased demagnetization coupling between the main-phase particles and a lower coercivity of the magnetic powder. In Fig. 2b, c, the white particles of the main-phase particles of $Nd_2Fe_{14}B$ successively decrease in size and number, indicating that tempering has facilitated the diffusion of Nd into the magnetic powder. This suggests that tempering provides a driving force for atomic diffusion, allowing Nd to diffuse to more grain boundaries, thereby enhancing the demagnetization coupling effect and increasing the coercivity of the magnetic powder. Figure 2d, e depicts the enlargement of $Nd_2Fe_{14}B$ main-phase particles and the appearance of larger white Nd-rich particles on the surface, which is attributed to the abnormal growth of $Nd_2Fe_{14}B$ main-phase particles and the precipitation of Nd-rich particles due to the high tempering temperature, leading to a reduction in the coercivity of the magnetic powder. The sticking phenomenon of $Nd_2Fe_{14}B$ main-phase grains in Fig. 2f is due to the fact that the tempering temperature is much larger than the melting point of the Nd-rich phase of 650–700 ℃, which accelerates the flow of the Nd-rich phase in liquid state.

Figure 3 shows the variation curves of the magnetic properties of the magnetic powders at a tempering temperature of 650 °C and tempering times of 10, 20, 30, 40, and 50 min; from Fig. 3, it can be observed that the remanent magnetization of the magnetic powder decreases,

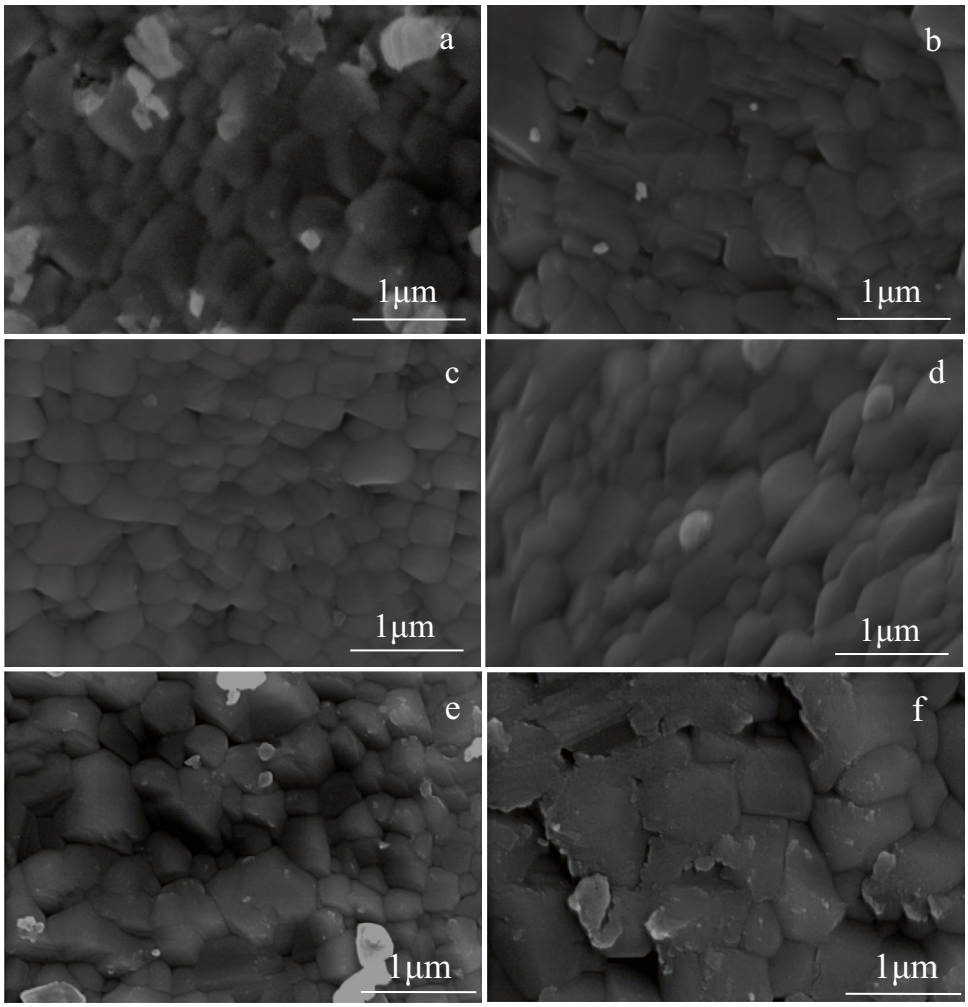

Fig. 2 SEM photos of magnetic powder with tempering time of 20 min and different tempering temperatures: **a** untempered, **b** 600 ℃, **c** 650 ℃, **d** 700 ℃, **e** 750 ℃, and **f** 800 ℃

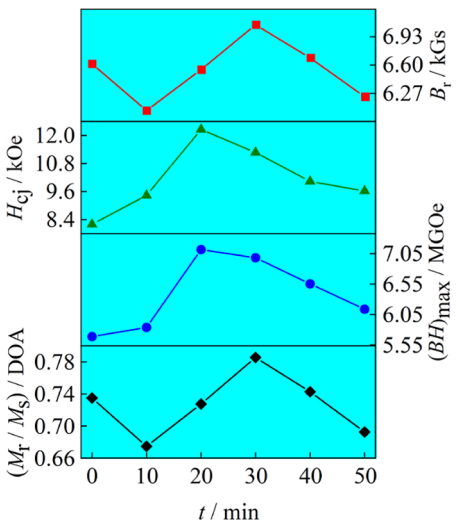

Fig. 3 Magnetic property change curve of magnetic powder under different tempering time

then increases, and then decreases again with the increase in tempering time. The coercivity of the magnetic powder increases and then decreases as the tempering time increases. The initial increase is attributed to the full diffusion of Nd energy on the grain surface to achieve the effect of demagnetization coupling, thereby improving the coercivity of the magnetic powder. Subsequently, the decrease is due to the prolonged tempering time, leading to potential adhesion between the main phase particles, an increase in particle size, reduced grain boundary numbers, weakened demagnetization coupling effects, and decreased coercivity of the magnetic powder. The maximum magnetic energy product of the magnetic powder increases and then decreases with the increase in tempering time, while the anisotropic orientation of the magnetic powder first decreases, then increases, and then decreases again. In summary, the coercivity of the magnetic powder is maximum at a tempering time of 20 min, and its ideal integrated magnetic properties are DOA = 0.73, B_r = 6.547 kGs, H_{cj} = 12.255 kOe, and $(BH)_{max}$ = 7.117 MGOe.

Figure 4a–f depicts the SEM photographs of untempered and the magnetic powders at a tempering temperature of 650 °C and tempering times of 10, 20, and 30 min. From Fig. 4a to c, the spaces within the $Nd_2Fe_{14}B$ main phase grains become smaller and clearer, and the number and size of the white Nd-rich grains on the surface sequentially decrease. This occurrence is attributed to the fact that tempering provides a driving force for the diffusion of the grains, resulting in the diffusion of Nd-rich grains into the grain boundaries or corners to enhance the demagnetization coupling and improve the coercivity of the magnetic powder. In Fig. 4d–f, the $Nd_2Fe_{14}B$ main phase grain size abnormally grows, leading to the adhesion phenomenon, causing some of the Nd precipitation at the grain boundaries to be distributed on the surface of the main-phase grains. Consequently, the demagnetization coupling effect decreases, resulting in a reduction in the coercive force of the magnetic powder.

Based on the above analysis, the ideal tempering temperature and time of are 650 °C and 20 min, respectively. Utilizing these parameters, the magnetic powders prepared under the conditions of HD at a temperature of 820 °C and DR at a temperature of 860 °C underwent the tempering process to enhance the magnetic properties of the magnetic powders.

Figure 5 depicts the comparison curves of the magnetic properties of tempered untempered magnetic powders after tempering at 650 °C for 20 min. It is evident that tempering the magnetic powders at appropriate temperatures times can effectively increase the remanent magnetization, coercivity, magnetic energy product, and DOA of the powders. A higher degree of anisotropic orientation (DOA) indicates a greater tendency for the grain orientations of the major phases of the $Nd_2Fe_{14}B$ to be consistent. The increase in coercivity is attributed to the expansion of the magnetic energy area and DOA of the magnetic powder facilitated by the tempering heat treatment under suitable process parameters. This process promotes the diffusion of atoms, facilitating the diffusion of Nd from the Nd-rich phase region to the low concentration Nd phase region of the grain boundary. This maximizes the distribution range of Nd-rich phases at the grain boundary, reinforcing the pinning effect on the movement of the magnetic domains, enhancing the effect of demagnetization coupling, and improving the comprehensive magnetic

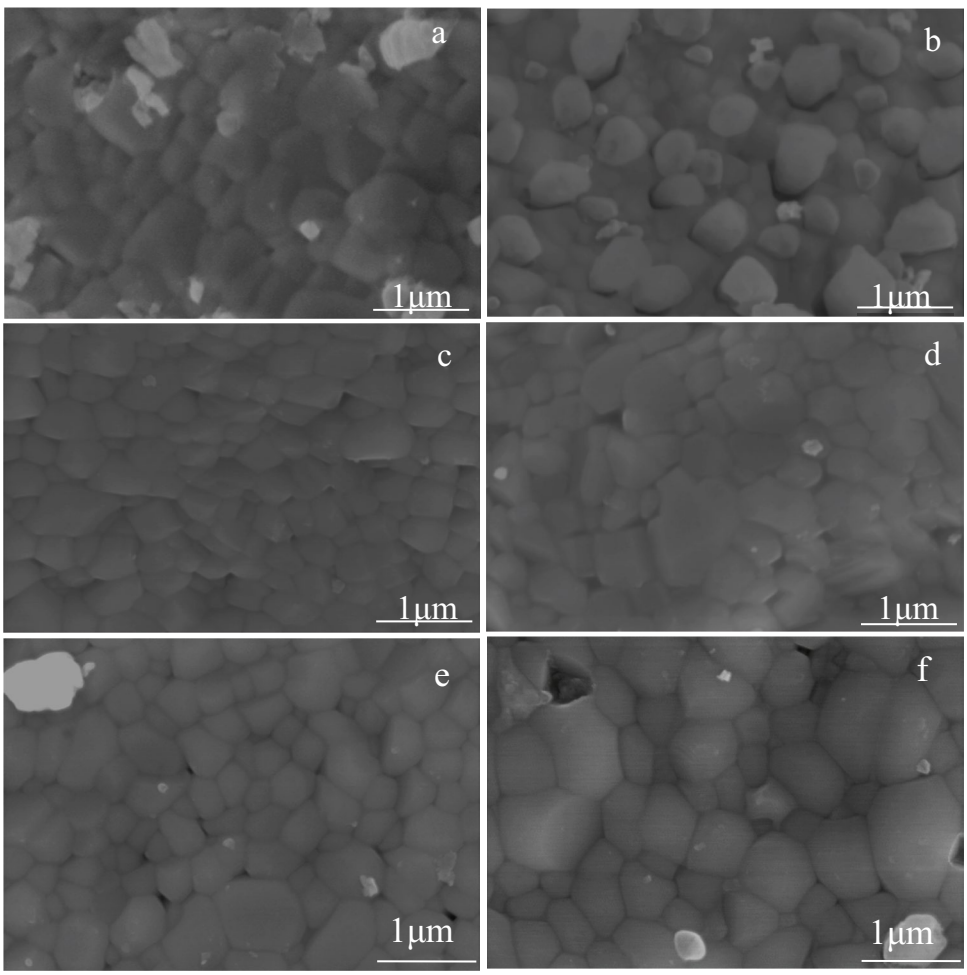

Fig. 4 SEM photos of magnetic powder with tempering temperature of 650 °C and different tempering times: **a** untempered, **b** 10 min, **c** 20 min, **d** 30 min, **e** 40 min, and **f** 50 min

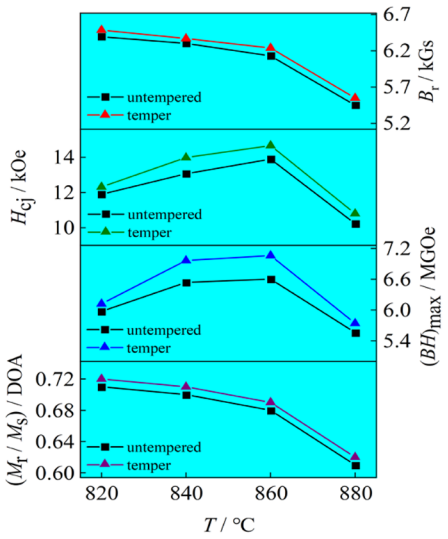

Fig. 5 Comparison of the magnetic property curves of the initial sample and the heat-treated magnetic powder tempered at 650 ℃ for 20 min

properties of the magnetic powders. The optimum combined magnetic properties of the magnetic powders were attained with a DOA = 0.69, B_r = 6.24 kGs, H_{cj} = 14.67 kOe, and $(BH)_{max}$ = 7.06 MGOe.

Based on Table 1, it can be observed that the coercivity of the magnetic powder in this study, after undergoing annealing treatment, is higher than that of the magnetic powder or magnets in previous studies after annealing. However, there still exists a certain gap in terms of residual magnetism and magnetic energy product.

3.2 Effect of Ball Milling on the Structure and Magnetic Properties of Nd-Fe-B Magnetic Powder

In the previous section, we improved the microstructure and magnetic properties of Nd-Fe-B magnetic powder through tempering heat treatment. However, there is still a considerable amount of large particle size, approximately 1 μm, and the magnetic properties of the magnetic powder could potentially be further enhanced. Therefore, in the following section, we investigate the effect of ball milling treatment on the organization of the magnetic powder and its magnetic properties.

Figure 6 depicts the comparative magnetic energy curves of magnetic powders 2 h of ball milling at speeds of 150 rpm, 250 rpm, 350 rpm, and 450 rpm. From the Fig. 6, it is observed that the remanent magnetization increases and then decreases with the increase of ball milling speed. When the ball milling speed reaches 350 rpm and 450 rpm, the remanent magnetization decreases below the initial sample due to the destruction caused by the excessively high milling speed. The coercivity increases first and then decreases. The first increase is because ball milling can make the Nd-rich phase and the main phase grains uniformly refined and improve the degree of anisotropic orientation of the magnetic powder, and at the same time provide energy for atomic diffusion, which is conducive to the uniform distribution of Nd in the grains or between the grain clusters, so the coercive force increases. The subsequent decrease in coercivity is attributed to the excessive energy provided by the high ball milling speed, with a portion being converted into heat. This leads to the recombination of dispersed grains and a reduction in the coercivity of the magnetic powder. The magnetic energy product and the degree of anisotropic orientation of the magnetic powder initially increase and then decrease with the ball milling speed. In summary, the coercivity of the magnetic powder is maximum at a ball milling speed of 250 rpm, and its ideal integrated magnetic properties are DOA = 0.55, B_r = 4.93 kGs, H_{cj} = 7.23 kOe, and $(BH)_{max}$ = 3.23 MGOe.

Table 1 Comparison table of magnetic properties for different tempering process parameters

Sample condition	Tempering parameters	H_{cj}/kOe	References
Sintered NdFeB	900℃ 2 h and 600℃ 3 h	13.63	[19]
Sintered NdFeB	450℃ 3.5 h	12.45	[20]
NdFeB magnetic powder	700℃ 30 min	12.31	[21]
NdFeB magnetic powder	650℃ 20 min	14.67	The study

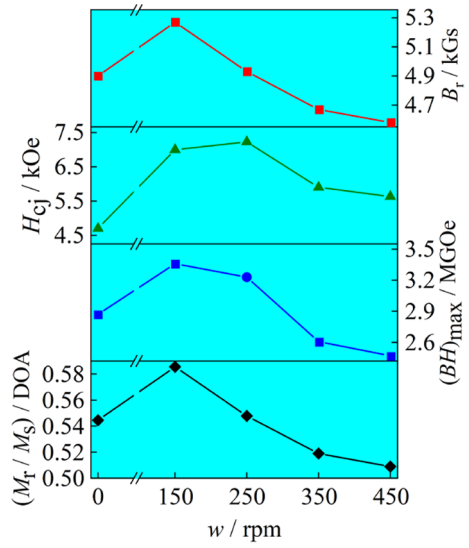

Fig. 6 Comparison of magnetic curves of magnetic powders prepared at different ball milling speeds

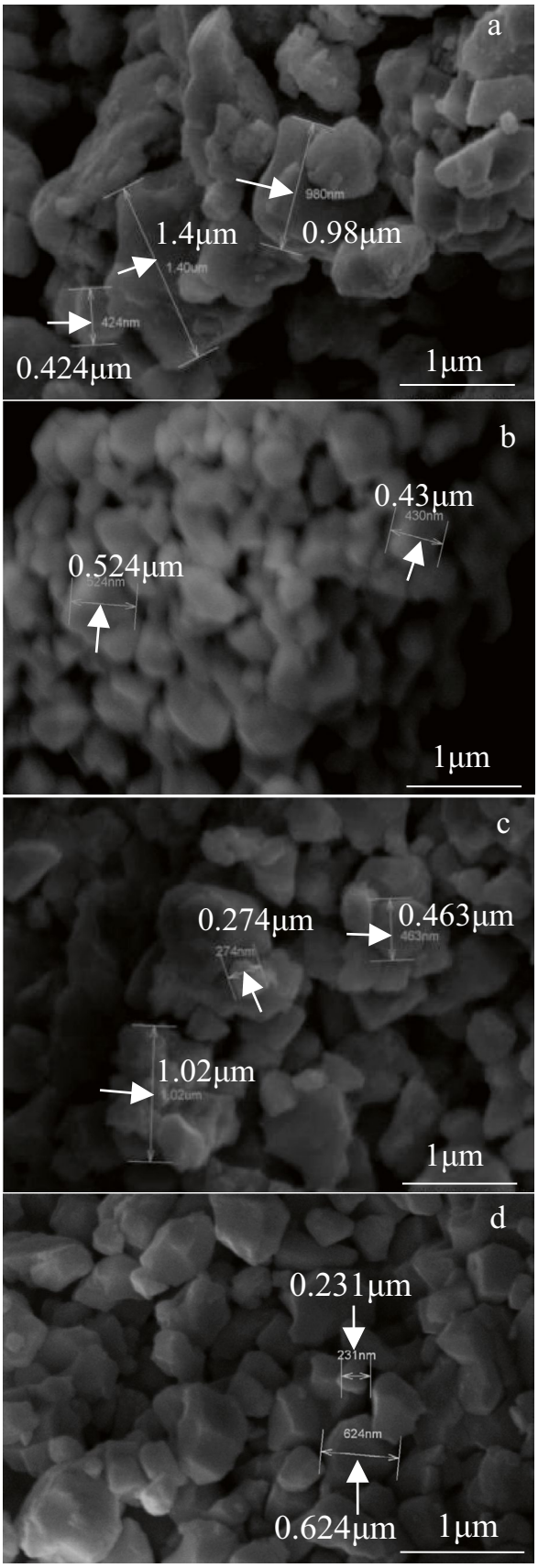

Fig. 7 SEM photos of magnetic powders at different ball milling speeds for 2h ball milling time. **a** 150 rpm, **b** 250 rpm, **c** 350 rpm, and **d** 450 rpm

Figure 7 presents the scanning electron micrographs of the magnetic powders under the conditions 2 h of ball milling at speeds of 150 rpm, 250 rpm, 350 rpm, and 450 rpm. In Fig. 7a, the particle size of the magnetic powder remains large and is hardly reduced. Conversely, in Fig. 7b, the particle size of the magnetic powder is reduced to 0.4–0.5 μm, which approximates the single domain grain size of 0.3–0.5 μm and exhibits uniform particle sizes. In Fig. 7c, d, some of the magnetic powders feature particle sizes smaller than that of the single domain grain size, while others have grown abnormally due to the high ball milling speed and energy, leading to an increase in thermal energy causing the dispersed particles to recombine and reagglomerate. The analysis indicates that none of the magnetic powders show noticeable Nd-rich phase particles after ball milling. Instead, they are uniformly distributed between the $Nd_2Fe_{14}B$ main phase grains, forming an ideal nonmagnetic grain boundary phase that enhances the coercivity of the magnetic powders.

Figure 8 depicts the comparative magnetic curves of the magnetic powders ball milling for 1, 2, 3 and 4 h at a ball milling speed of 250 rpm. It can be observed that with an increase in the ball milling time, the remanent magnetization initially decreases and then increases. Similarly, the coercivity initially increases and then decreases. The initial increase in coercivity is attributed to the uniform refinement of the main phase grains and Nd-rich phase particles, enabling the refined Nd-rich phase particles to be uniformly distributed in the grains or clusters of grains, thereby enhancing the coercivity of the magnetic powder. The subsequent decline is due to the excessive energy provided by the long ball milling time, some of which is converted to heat. This leads to the reagglomeration of dispersed particles, resulting in a reduction in the coercivity of the magnetic powder. Additionally, with an increase in ball milling time, the magnetic energy product and the degree of anisotropic orientation initially increase and then decrease. In summary, the coercivity of magnetic powder is maximum at a ball milling time of 2 h, and its ideal integrated magnetic properties are DOA = 0.55, B_r = 4.93 kGs, H_{cj} = 7.23 kOe, and $(BH)_{max}$ = 3.23 MGOe.

Figure 9a–c displays the SEM photographs of the powders after undergoing ball milling for 1, 2, and 3 h at a speed of 250 rpm. In Fig. 9a, some large grains with non-uniform particle size can still be observed. In Fig. 9b, the particle size of the magnetic powder is reduced to 0.4–0.5 μm, closely matching the single-domain particle size of 0.3–0.5 μm and exhibiting uniform particle size. In Fig. 9c, d, some of the magnetic powders show a slight reduction in particle size, while others begin to display signs of agglomeration and

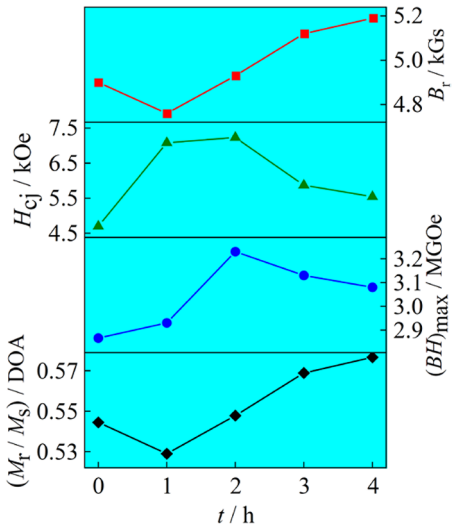

Fig. 8 Comparison of magnetic curves of magnetic powders prepared at different milling times

adhesion. This phenomenon is a result of prolonged ball milling, where the continuing high energy, with some being converted into heat, causes dispersed particles to reunite. The extended ball milling time and the sustained high energy result in recombination and dispersion of particles.

Figure 10 illustrates the comparison curves of the magnetic properties of magnetic powders doped with 5 wt%, 10 wt%, and 15 wt% Cu powders, which were treated with 2 h of ball milling at a speed of 250 rpm. The trend of remanent magnetization, magnetic energy product, and degree of anisotropic orientation is not apparent with the increase of Cu doping, and the coercive force initially increases and then decreases. In summary, the magnetic powder has the highest coercivity when doped with 10 wt% Cu powder, and its ideal integrated magnetic properties are DOA = 0.62, B_r = 4.96 kGs, H_{cj} = 9.86 kOe, and $(BH)_{max}$ = 4.39 MGOe.

Figure 11 displays the XRD pattern of the initial magnetic powder doped with 10 wt% Cu powder after ball milling. From Fig. 11, it is evident that this XRD pattern aligns well with the PDF cards of $Nd_2Fe_{14}B$ and Cu, indicating that the magnetic powder mainly comprises the main phase of.

$Nd_2Fe_{14}B$ and Cu elements show no signs of oxides, Table 2 demonstrating that the experiments were conducted under good vacuum conditions without oxidation, and no other phases were detected.

Figure 12 illustrates the Rietveld fine-fit comparison of powders doped with different concentrations of Cu powder. The figure indicates that the content of the $Nd_2Fe_{14}B$ main phase decreases with higher Cu doping levels, while the content of Nd-rich phase gradually increases. Notably, when doped with 15 wt% Cu powder, the increased presence of the Nd-rich phase leads to excessive consumption

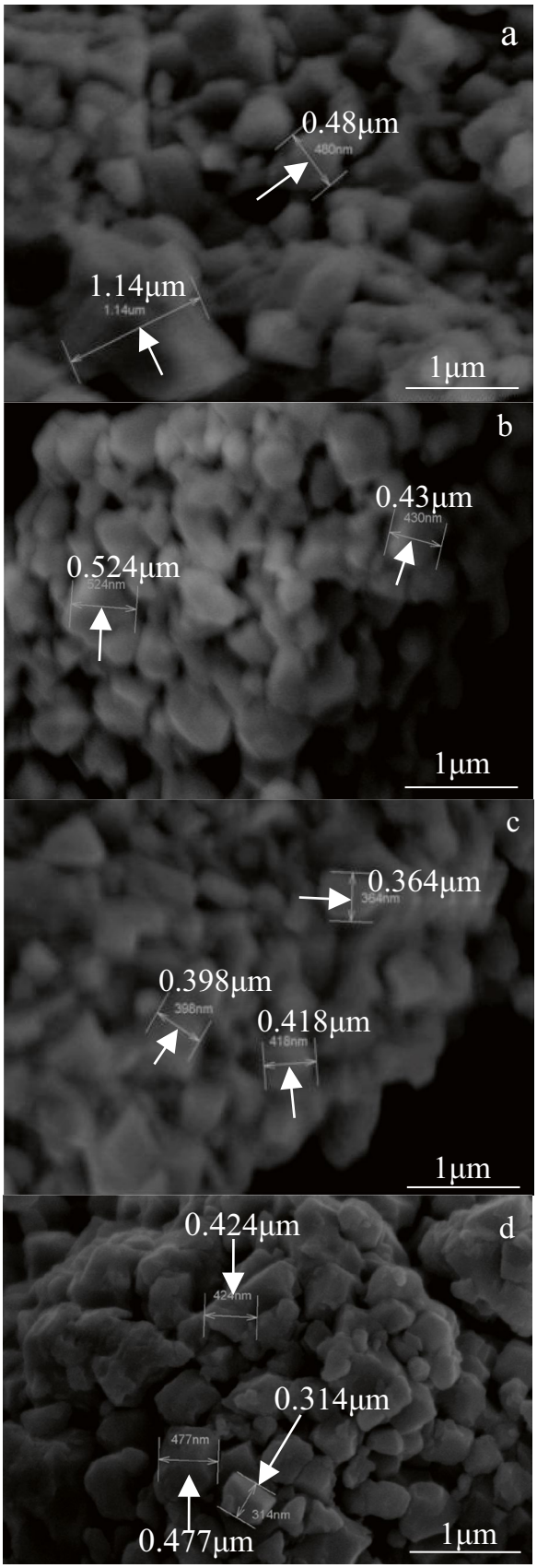

Fig. 9 SEM photos of magnetic powder at 250rpm ball milling speed and different ball milling time. **a** 1 h, **b** 2 h, **c** 3 h, and **d** 4 h

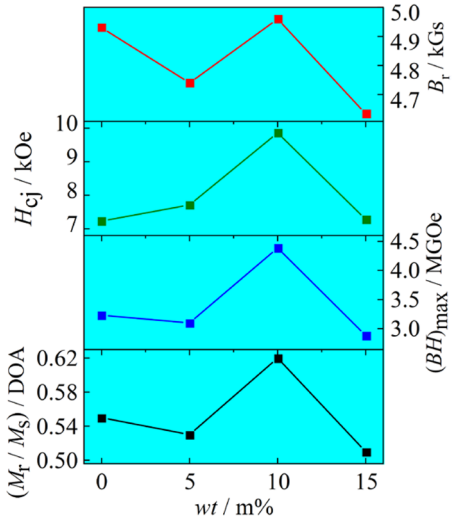

Fig. 10 Comparison of magnetic curve of magnetic powder prepared by ball milling doped with different Cu content

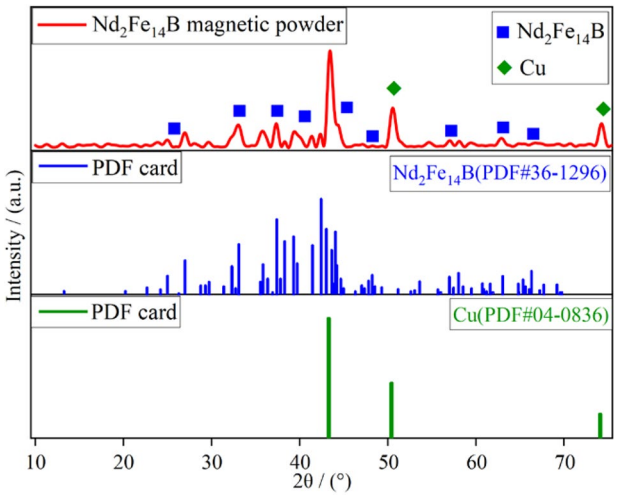

Fig. 11 XRD pattern of magnetic powder prepared by ball milling doped with 10wt% Cu powder

Table 2 Rietveld refined and fitted magnetic powder composition comparison table

Cu content/ wt%	$Nd_2Fe_{14}B$	Nd	Cu
5	98.2	1.5	0.3
10	98.1	1.6	0.3
15	97.8	1.9	0.3

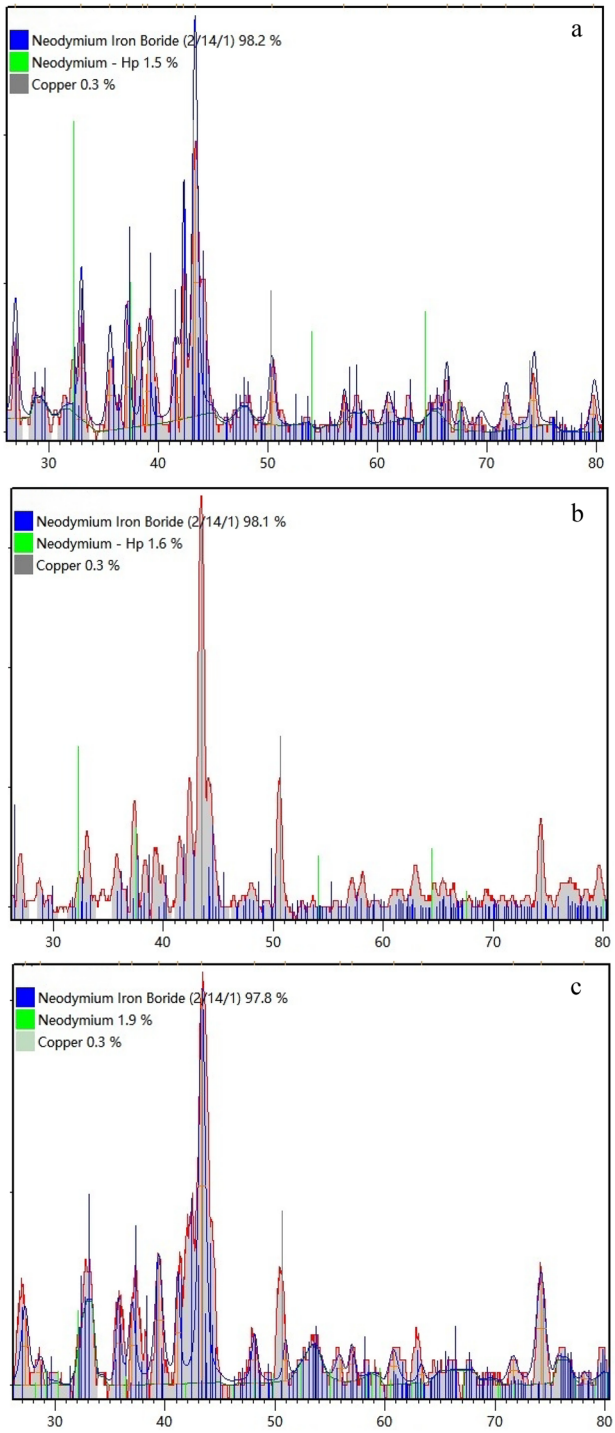

Fig. 12 Rietveld finishing fitting comparison of magnetic powders prepared by ball milling doped with different contents of Cu powder. **a** 5 wt%, **b** 10 wt%, and **c** 15 wt%

of $Nd_2Fe_{14}B$ main phase grains and a rise in the non-magnetic phase within the magnetic powder. Consequently, this diminishes the coercivity and remanent magnetization of the magnetic powder. Analytically, the results indicate that doped Cu can induce the precipitation of a certain amount of Nd atoms from the $Nd_2Fe_{14}B$ main phase during the ball milling process. These atoms are uniformly distributed at the grain boundaries of the grains or grain clusters, suggesting that Cu has a grain boundary repair effect.

4 Conclusions

In this study, the ideal process parameters and magnetic properties were obtained by tempering and ball milling processes with the objective of maximizing the coercivity. Specific analyses in conjunction with characterization tests yielded the following results.

1. The tempering process with appropriate temperature and time can promote the diffusion of Nd-rich phases, increase the content of Nd-rich at the grain boundaries of grains or grain clusters, strengthen the demagnetization coupling effect, and improve the coercivity of the magnetic powder. When the tempering temperature is 650 °C and the tempering time is 20 min, the coercivity of the magnetic powder is maximum, and its ideal magnetic properties of the magnetic powder are DOA = 0.73, B_r = 6.547 kGs, H_{cj} = 12.255 kOe, and $(BH)_{max}$ = 7.117 MGOe. When the DR temperature is 860 °C, the tempering temperature is 650 °C, and the tempering time is 20 min, the ideal magnetic properties of the magnetic powder are DOA = 0.69, B_r = 6.238 kGs, H_{cj} = 14.67 kOe, and $(BH)_{max}$ = 7.060 MGOe.
2. The ball milling process can uniformly refine the particle size of the main phase grains and Nd-rich phase particles in the magnetic powder and increasing the degree of anisotropic orientation of magnetic powder, resulting in the uniform distribution of the Nd-rich phase between the grains of the main phase $Nd_2Fe_{14}B$ to form an ideal non-magnetic grain boundary phase. This strengthens the effect of demagnetization coupling and improves the coercive force of the magnetic powder. Additionally, doped Cu can induce the precipitation of a certain amount of Nd from the $Nd_2Fe_{14}B$ main phase, which is then uniformly distributed on the grain boundaries of the grains or grain clusters to enhance the effect of demagnetization coupling and improve the coercivity of the magnetic powder. When the ball milling speed is 250 rpm and the time is 2 h, the coercivity of the magnetic powder is maximum, and its ideal magnetic energy is DOA = 0.55, B_r = 4.93 kGs, H_{cj} = 7.23 kOe, and $(BH)_{max}$ = 3.23 MGOe. Furthermore, based on this process, the coercivity of the magnetic powder is maximum when doped with 10 wt% Cu, and its ideal combined magnetic properties are DOA = 0.62, B_r = 4.96 kGs, H_{cj} = 4.96 kGs, and $(BH)_{max}$ = 4.39 MGOe.

Acknowledgements I am grateful to Mingang Zhang, Fenghua Chen, Wenfeng Liu, and Yongan Dong for many valuable discussions and comments.

Author Contributions Chao Liang's contributions: designing the research proposal, implementing the research process, reviewing related literature, collecting and organizing data and writing the article. The contributions of Mingang Zhang: proposing the research topic, directing the experimental process, directing the article writing, and obtaining the research grant. Fenghua Chen's contribution: guiding the experimental process, guiding the article writing. Contributions of Wenfeng Liu: supervised the writing of the article and obtained financial support for the research. Contribution of Yongan Dong: Provided raw materials for ingot NdFeB casting and experimental equipment for hydrogen crushing furnace, as well as the implementation of the research site. Many thanks to all the authors who contributed to this article.

Funding This work is supported by Shanxi Key R&D Program Project (201903D121086), Shanxi Collaborative Innovation Center for Advanced Permanent Magnet Materials and Technology Project (2019–01), and the Doctoral Starting-up Foundation of Taiyuan University of Science and Technology (No. 20192016).

Data Availability No datasets were generated or analyzed during the current study.

Declarations

Competing Interests The authors declare no competing interests.

References

1. Yang, L., Zhen, L., Xu, C.Y., et al.: Effects of proton irradiation on structure of NdFeB permanent magnets studied by X-ray diffraction and X-ray absorption fine structure[J]. J. Magn. Magn. Mater. **323**(1), 4–6 (2011)
2. Patil, D.R., Lee, S., Atul, T., et al.: Boosting the energy harvesting performance of cantilever structured magneto-mechano-electric generator by controlling magnetic flux intensity on magnet proof mass[J]. J. Mater. **9**(4), 735–744 (2023)
3. Pei, Y., Chen, F., Ma, T., et al.: An experimental investigation on the performance of novel NdFeB-based composite material for magnetic encoding of road environment information[J]. Mater. Today Commun. **36**, 106760 (2023)
4. Sun, R., Zheng, J., Zheng, B., et al.: New magnetic rails with double-layer Halbach structure by employing NdFeB and ferrite magnets for HTS maglev[J]. J. Magn. Magn. Mater. **445**, 44–48 (2018)
5. Mu, L., Priyo, S.: Suprapedi, Preparation and characterization of 5wt.% epoxy resin bonded magnet NdFeB for micro generator application[J]. Energy Procedia **68**, 282–287 (2015)
6. Zhou, S., Dong, Q.: Ultra-strong permanent magnet[M]. Metallurgical Industry Press, Beijing (2004)
7. Awais, I., Farhan, M., Richard, S.S., et al.: Particle size dependent sinterability and magnetic properties of recycled HDDR Nd–Fe–B powders consolidated with spark plasma sintering[J]. J. Rare Earths **38**(1), 90–99 (2020)

8. Nlebedim, I.C., Huseyin, U., Christine, B.H., et al.: Studies on in situ magnetic alignment of bonded anisotropic Nd-Fe-B alloy powders[J]. J. Magn. Magn. Mater. **422**, 168–173 (2017)
9. Zhai, Z.: "Tempering process for sintered NdFeB permanent magnets" validated in the U.S[N]. Science Review, A01, (2015). https://www.doc88.com/p-1877561826093.html
10. Ji, M., Wang, Z., Liu, W., et al.: Effect of grain boundary diffusion of terbium on mode of mechanical fracture of sintered NdFeB magnets[J]. J. Alloy. Compd. **970**, 172598 (2024)
11. Zhou, T., Bao, W., Xu, Z., et al.: Optimizing microstructure, magnetic properties and mechanical properties of sintered NdFeB magnet by double alloy method and grain boundary diffusion[J]. Intermetallics **162**, 108027 (2023)
12. Lu, Z., Wang, T., Jiang, J., et al.: Effect of grain boundary diffusion of terbium on mode of mechanical fracture of sintered NdFeB magnets[J]. J. Rare Earths **3**, 22 (2023)
13. Zhang, F., Liu, Y., Li, J., et al.: Ultrafine nanocrystalline NdFeB prepared by cryomilling with HDDR process[J]. J. Alloy. Compd. **750**, 401–408 (2018)
14. Sheridan, R., Williams, A., Harris, I., et al.: Improved HDDR processing route for production of anisotropic powder from sintered NdFeB type magnets[J]. J. Magn. Magn. Mater. **350**, 114–118 (2014)
15. Thompson, P., Gutfleisch, O., Chapman, N., et al.: A comparison of the micromagnetic and microstructural properties of four NdFeB-type materials processed by the HDDR route[J]. J. Magn. Magn. Mater. **202**(1), 53–61 (1999)
16. Wong, Y.J., Lin, B.S., Chang, H.W., et al.: Enhancement of coercivity and thermal stability of $Pr_{85}Al_{15}$ doped NdFeB sintered magnets followed with grain boundary diffusion[J]. J. Magn. Magn. Mater. **571**, 170562 (2023)
17. Zhou, T., Liu, Q., Lu, X., Pan, W., et al.: Microstructure modification and coercivity enhancement of sintered NdFeB magnet by vacuum diffusion 70Tb–20Cu–10Ga (at%) alloys[J]. Vacuum **212**, 112022 (2023)
18. Luo, S., Lu, Y., Zou, Y., et al.: Effect of low melting point powder doping on the properties and microstructure of sintered NdFeB magnets[J]. J. Magn. Magn. Mater. **523**, 167620 (2021)
19. Yu, L.Q., Zhang, Y.P., Zhong, X.L.: Effect of high temperature 900 ℃ tempering on magnetic properties of NdFeB[J]. Rare Metal Mat. Eng. **41**(1), 157–160 (2012)
20. Song, Q.: Effect of composition and tempering process on the organization and magnetic properties of sintered Nd-Fe-B[D]. Taiyuan University of Technology. (2020). https://cdmd.cnki.com.cn/Article/CDMD-10112-1020368868.htm
21. Yue, M., Liu, X., Xiao, Y., et al.: Coercivity of HDDR-processed anisotropic $Nd_2Fe_{14}B$-based magnets[J]. Rare Metal Mat. Eng. **7**, 490–493 (2003)
22. An, X., Jin, K., Abbas, N., et al.: High anisotropic NdFeB submicro/nanoflakes prepared by surfactant-assisted ball milling at low temperature[J]. J. Magn. Magn. Mater. **442**, 279–287 (2017)
23. Wang, L.: Preparation of Nd-Fe-B based magnetic powders by hydrothermal method and performance optimization[D]. Taiyuan University of Science and Technology. (2021). https://www.doc88.com/p-69716513434171.html
24. Hyundai, M.C.: System and method for manufacturing bonded magnets using rare earth powders[P]. CN201110456658. **X**, 04–03, (2013). https://d.wanfangdata.com.cn/patent/ChJQYXRlbnROZXdTMjAyMzA5MDESEENOMjAxMTEwNDU2NjU4LlgaCGgycjJndDd0
25. Hussain, M., Akram, R., Rafique, S., et al.: Microstructural and magnetic properties of cobalt-substituted $Nd_{32.5}Dy_{1.0}Fe_{64.2-x}Co_xNb_{1.0}Al_{0.2}B_{1.1}$ alloy prepared by ball milling technique[J]. Kuwait J. Sci. **50**(3), 238–243 (2023)
26. Liu, X.: Effect of tempering treatment on the structure and magnetic properties of sintered NdFeB magnets with added Dy_2O_3[J]. Hot Working Technology. **41**(16):168–171+174, (2012). http://www.doc88.com/p-0971411558037.html
27. Tan, C., Bai, S., Zhang, H., et al.: Effect of tempering treatment on the organization and magnetic properties of sintered NdFeB permanent magnetic materials[J]. Chin. J. Nonferrous Met. **S1**, 64–66 (2002)
28. Zhao, D.: Research on HDDR process of high performance NdFeB magnetic powder[D]. Taiyuan University of Science and Technology, Taiyuan (2020)
29. Liang, C., Zhang, M., Chen, F., et al.: Study of coercivity mechanism of anisotropic NdFeB alloys based on improved d-HDDR[J]. Magnetic Materials and Devices. **54**(02), 11–16 (2023)